Stem Cell Reports, Volume *17*

Supplemental Information

Human iPSC model reveals a central role for NOX4 and oxidative stress in Duchenne cardiomyopathy

Robin Duelen, Domiziana Costamagna, Guillaume Gilbert, Liesbeth De Waele, Nathalie Goemans, Kaat Desloovere, Catherine M. Verfaillie, Karin R. Sipido, Gunnar M. Buyse, and Maurilio Sampaolesi

SUPPLEMENTAL INFORMATION (Duelen et al.)

SUPPLEMENTAL ITEMS (FIGURES AND TABLES)

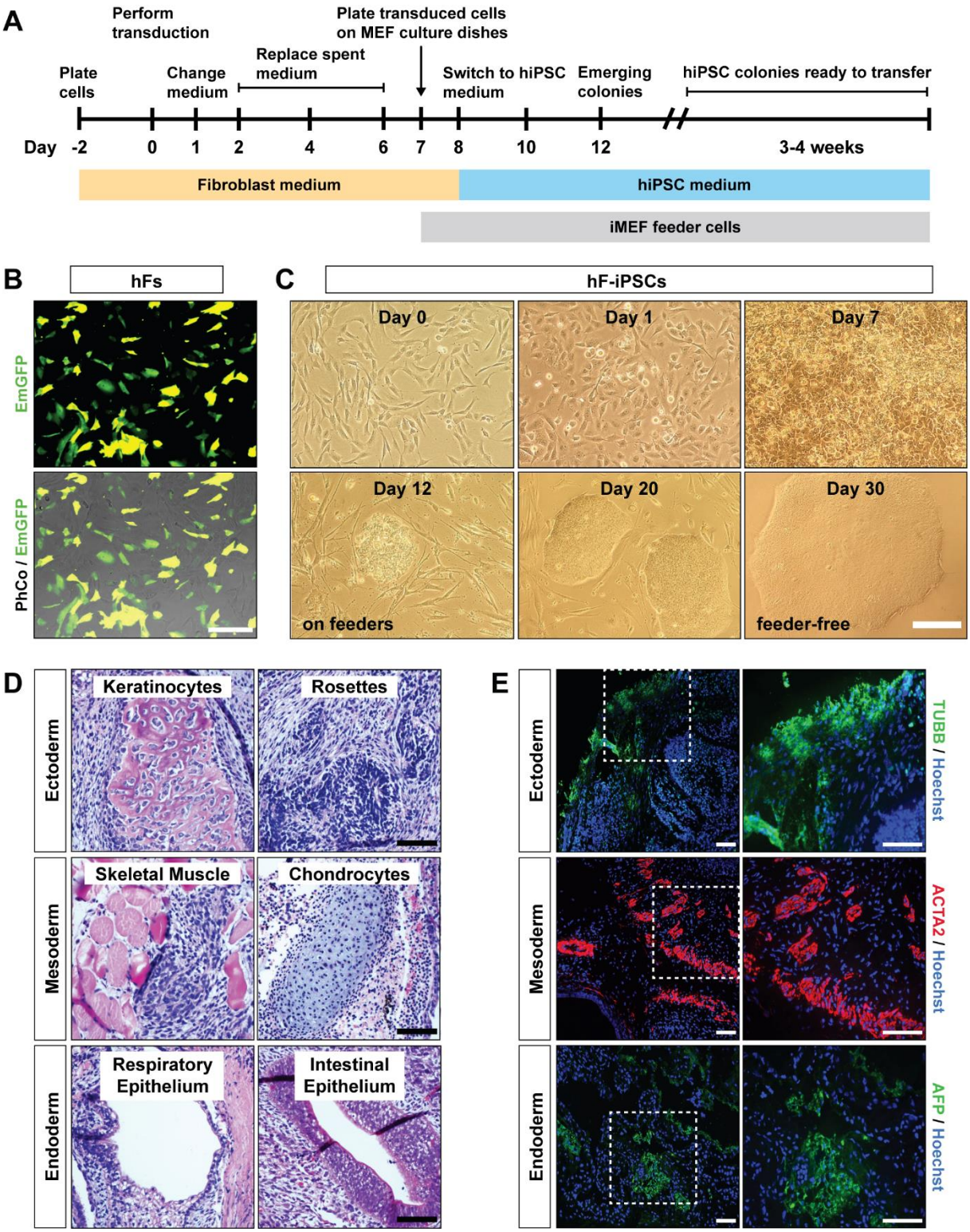

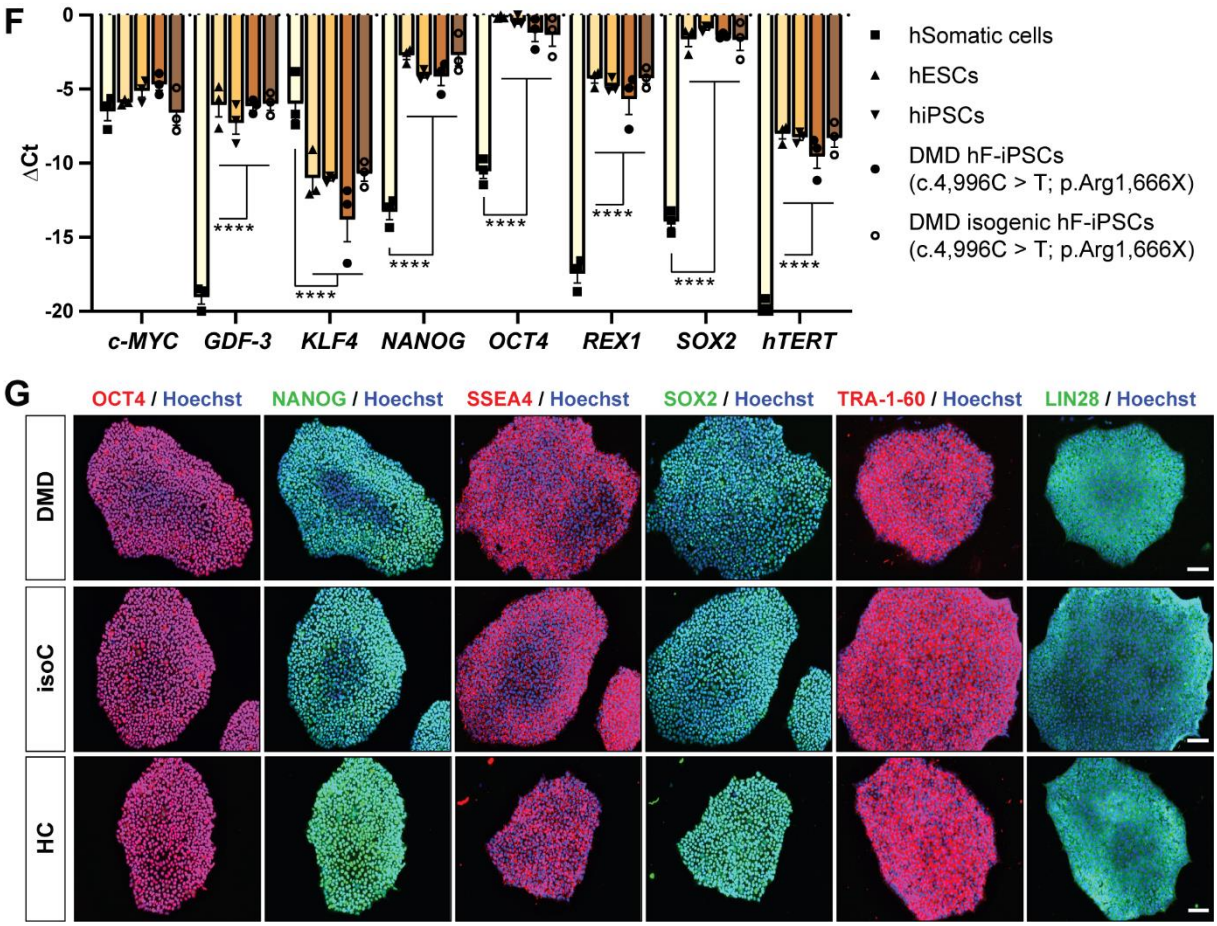

Fig. S1: Characterization of the SeV-mediated reprogrammed DMD patient hF-iPSC clones, harboring the nonsense mutation in exon 35 (c.4,996C > T; p.Arg1,666X) of the *Dystrophin* gene, and its CRISPR-Cas9 corrected DMD isogenic control line. (A) Schematic representation of the SeV hiPSC reprogramming protocol for hFs (data not shown for hPBMCs). hFs were transduced at day 0 using the integration-free SeV vectors, expressing the OSKM (OCT3/4, SOX2, KLF4 and c-MYC) pluripotency markers. **(B)** EmGFP (green) expression of transduced DMD somatic cells, 1 day after transduction with SeV reprogramming vectors. **(C)** Morphological progression of DMD hFs towards hiPSC clones. **(D)** Hematoxylin and eosin staining on SeV-reprogrammed hiPSC-induced *in vivo* teratomas showing the derivatives of the three developmental germ layers, including keratinocytes and rosettes (ectoderm), skeletal muscle fibers and chondrocytes (mesoderm), and epithelium from respiratory and intestinal tract (endoderm). **(E)** Immunostaining of three germ lineage markers: Beta Tubulin (TUBB; ectoderm), Alpha Smooth Muscle Actin (ACTA2; mesoderm) and Alpha Fetoprotein (AFP; endoderm). Scale bar = 100 μm. The pluripotency state of the DMD isogenic control line. The following pluripotency genes (*c-MYC, GDF-3, KLF4, NANOG, OCT4, REX1, SOX2* and *hTERT*) **(F)** and proteins (OCT4, NANOG, SSEA4, SOX2, TRA-1-60 and LIN28) **(G)** were analyzed. Human embryonic stem cell lines (hESCs) and commercially available undifferentiated hiPSC lines were used as positive controls. Each data point was represented as ΔCt, normalized for the housekeeping genes (*GAPDH, HPRT* and *RPL13a*). Data were representative of three independent experiments (n = 3) and values were expressed as mean ± SEM. Significance of the difference was indicated as follows: *p < 0.05; **p < 0.01; ***p < 0.001 and ****p < 0.0001. Scale bar = 100 μm.

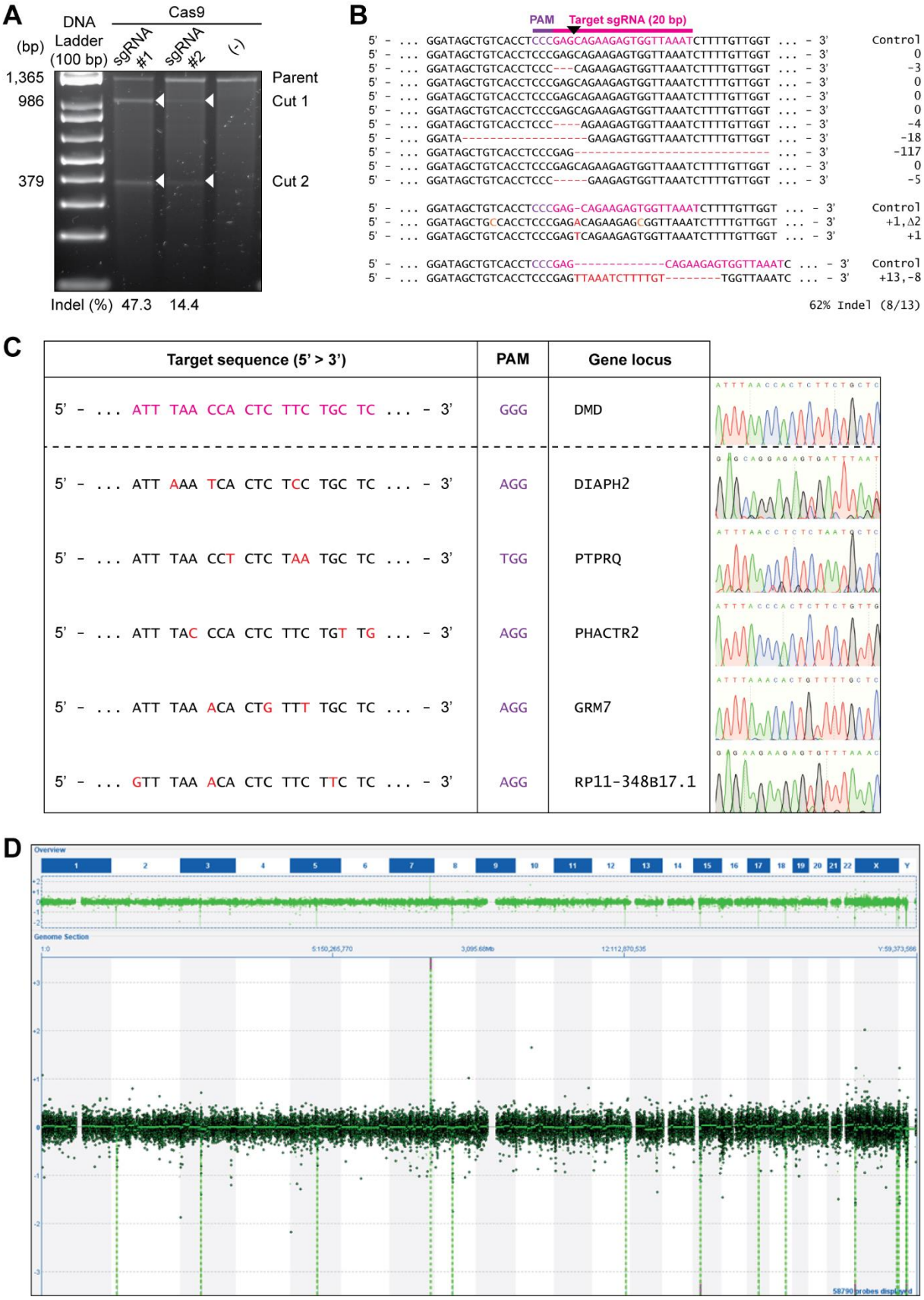

Fig. S2: Validation of the Cas9 cutting efficiency and analysis of the off-targets. (A) Surveyor assay in HEK293T cells to evaluate the cutting efficiency of the sgRNAs, represented as random events of base pair (bp) insertions or deletions (indel) after DSB. **(B)** DNA sequencing of the NHEJ events after transfection of the sgRNA-Cas9 plasmids in HEK293T cells. **(C)** List of CRISPR-Cas9 off-targets

(source: www.synthego.com). **(D)** Detailed CGH molecular karyotyping showing no additional chromosomal abnormalities due to unwanted Cas9-mediated DSB cuts.

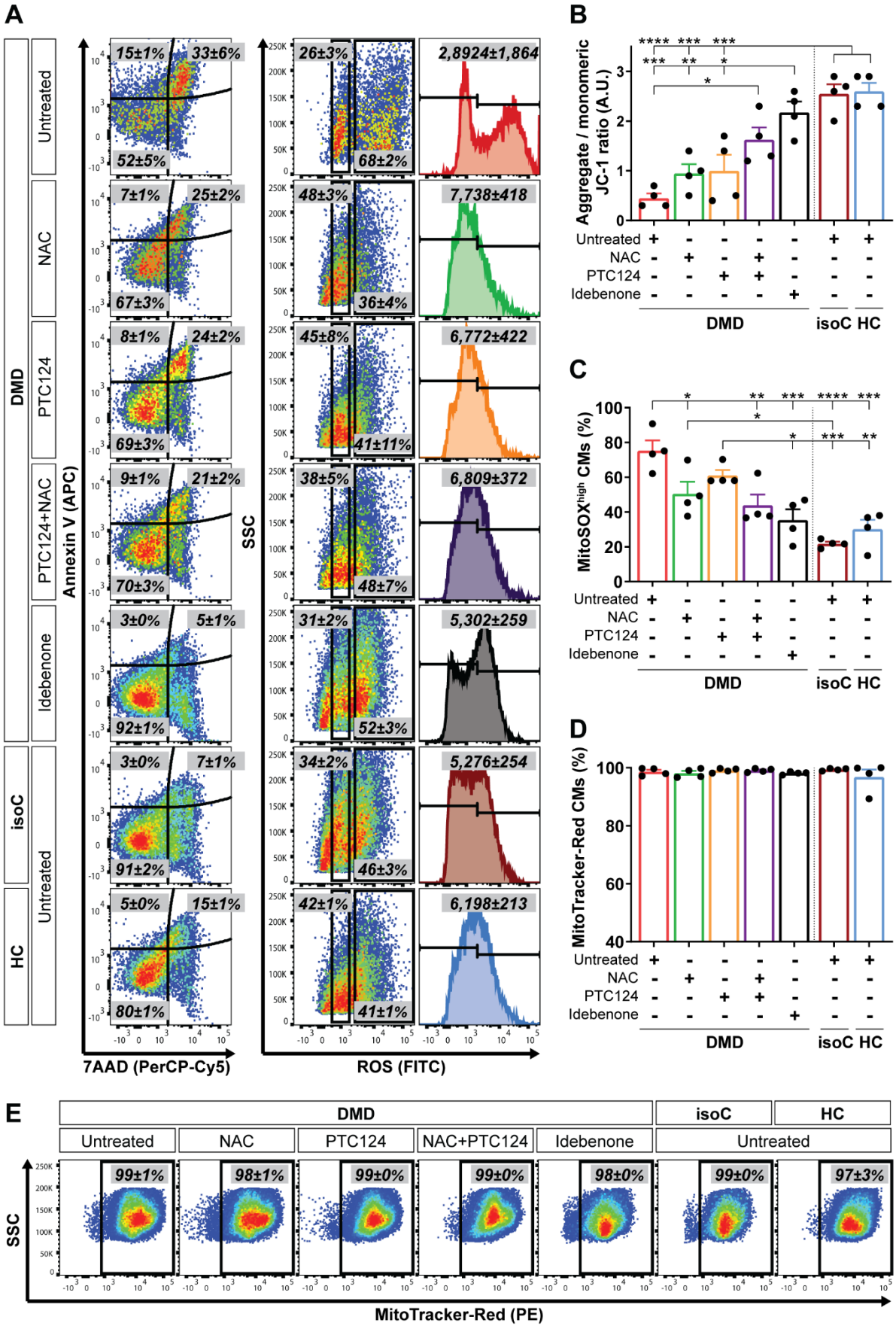

Fig. S3: Corresponding flow cytometric graphs and quantification for the characterization of the cardiomyopathic phenotype of DMD hiPSC-CMs, showing premature cell death, depolarized

mitochondria and increased intracellular ROS levels. (A) Representative flow cytometric analyses at day 15 of cardiac differentiation showing the percentage of cell death (using annexin V, APC and 7AAD, PerCP-Cy5, *left panels*) and intracellular ROS (FITC, *right panels*) in untreated and treated DMD hiPSC-CMs compared to the DMD isogenic and healthy controls. Human iPSC-CMs were stained for SIRPA (PE) to obtain high CM purity (data not shown). Flow cytometric quantification at day 15 of differentiation showing the JC-1 aggregates/monomers ratio **(B)** and the mitochondrial superoxide production (MitoSOX) in depolarized DMD mitochondria **(C)** compared to DMD isogenic and healthy controls. **(D)** Percentage of MitoTracker-Red positive CMs upon NAC, PTC124 and idebenone treatment. **(E)** Corresponding flow cytometric analyses of the percentage of MitoTracker-Red (PE) positive hiPSC-CMs. Data were representative of four independent experiments (n = 4). Data were reported as mean ± SEM; *p < 0.05; **p < 0.01; ***p < 0.001 and ****p < 0.0001.

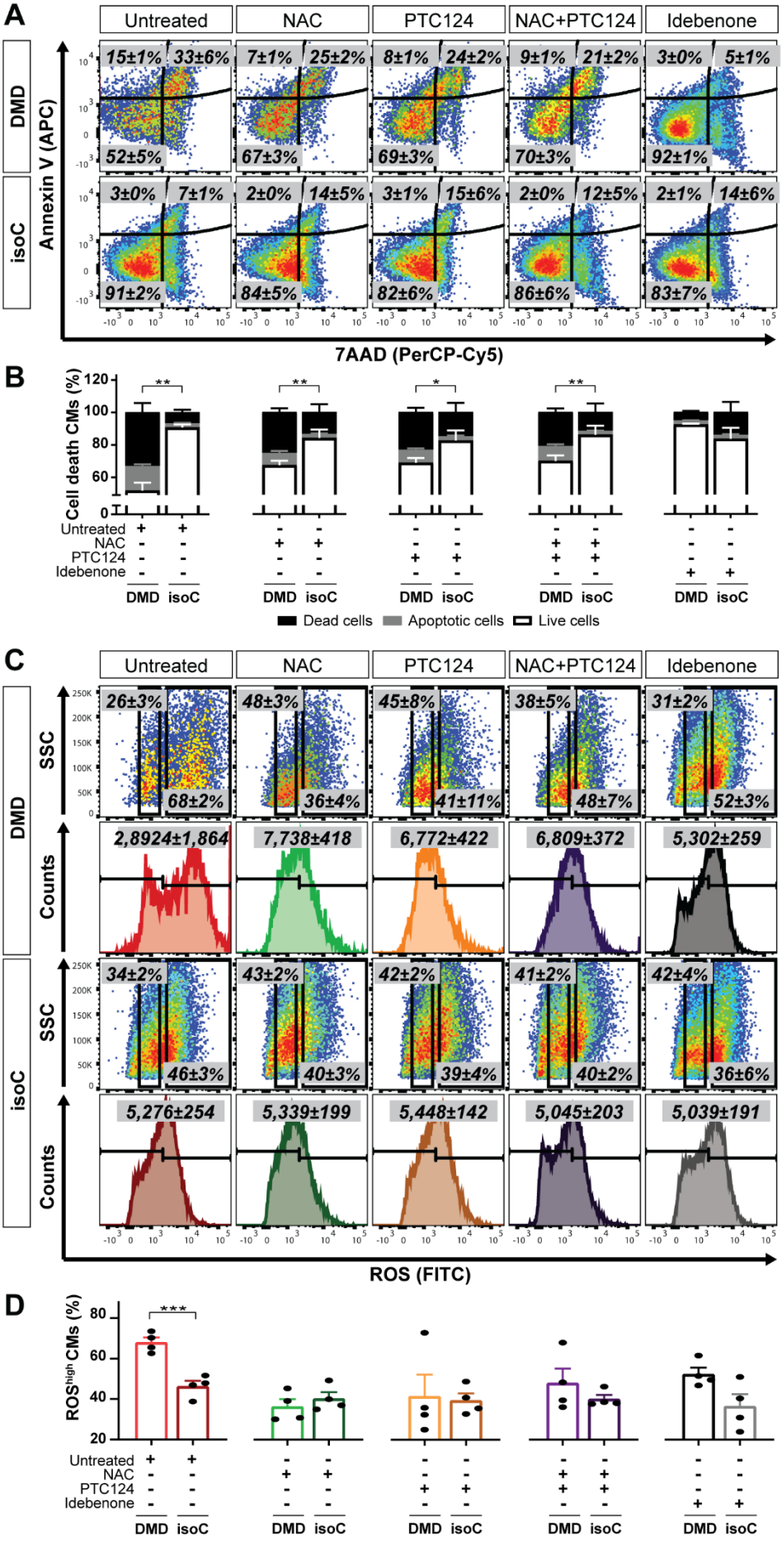
A
Untreated
NAC
PTC124
NAC+PTC124
Idebenone
DMD
isoC
Annexin V (APC)
7AAD (PerCP-Cy5)
15±1%
33±6%
7±1%
25±2%
8±1%
24±2%
9±1%
21±2%
3±0%
5±1%
52±5%
67±3%
69±3%
70±3%
92±1%
3±0%
7±1%
2±0%
14±5%
3±1%
15±6%
2±0%
12±5%
2±1%
14±6%
91±2%
84±5%
82±6%
86±6%
83±7%
B
Cell death CMs (%)
Untreated
NAC
PTC124
Idebenone
DMD
isoC
Dead cells
Apoptotic cells
Live cells
C
SSC
Counts
ROS (FITC)
26±3%
48±3%
45±8%
38±5%
31±2%
68±2%
36±4%
41±11%
48±7%
52±3%
2,8924±1,864
7,738±418
6,772±422
6,809±372
5,302±259
34±2%
43±2%
42±2%
41±2%
42±4%
46±3%
40±3%
39±4%
40±2%
36±6%
5,276±254
5,339±199
5,448±142
5,045±203
5,039±191
D
ROS^high CMs (%)

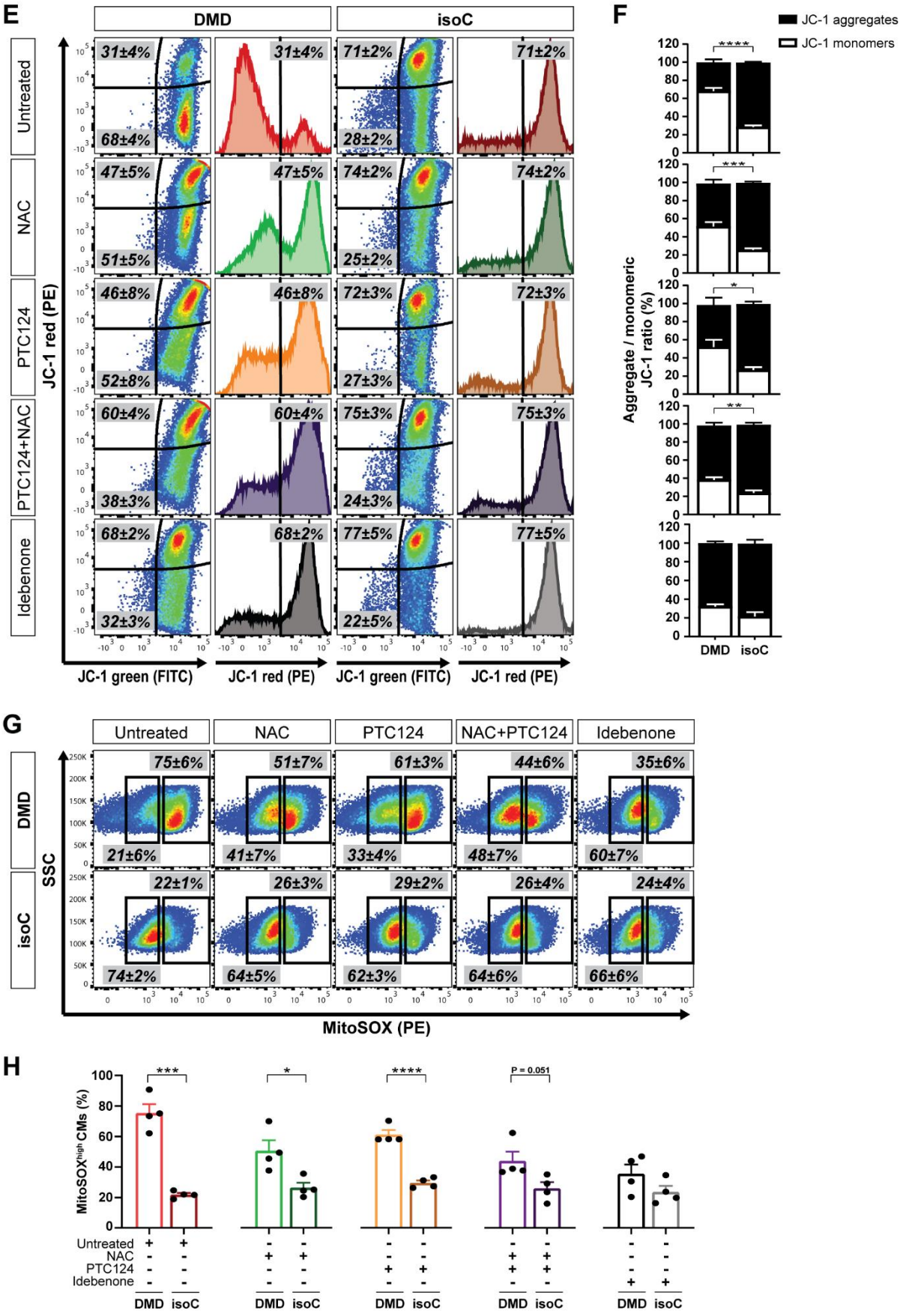
E
DMD
isoC
Untreated
NAC
PTC124
PTC124+NAC
Idebenone
JC-1 red (PE)
JC-1 green (FITC)
JC-1 red (PE)
JC-1 green (FITC)
JC-1 red (PE)
31±4%
68±4%
31±4%
71±2%
28±2%
71±2%
47±5%
51±5%
47±5%
74±2%
25±2%
74±2%
46±8%
52±8%
46±8%
72±3%
27±3%
72±3%
60±4%
38±3%
60±4%
75±3%
24±3%
75±3%
68±2%
32±3%
68±2%
77±5%
22±5%
77±5%
F
JC-1 aggregates
JC-1 monomers
Aggregate / monomeric JC-1 ratio (%)
****
***
*
**
DMD
isoC
G
Untreated
NAC
PTC124
NAC+PTC124
Idebenone
DMD
isoC
SSC
MitoSOX (PE)
75±6%
21±6%
51±7%
41±7%
61±3%
33±4%
44±6%
48±7%
35±6%
60±7%
22±1%
74±2%
26±3%
64±5%
29±2%
62±3%
26±4%
64±6%
24±4%
66±6%
H
MitoSOXhigh CMs (%)
***
*
****
P = 0.051
Untreated
NAC
PTC124
Idebenone
DMD
isoC

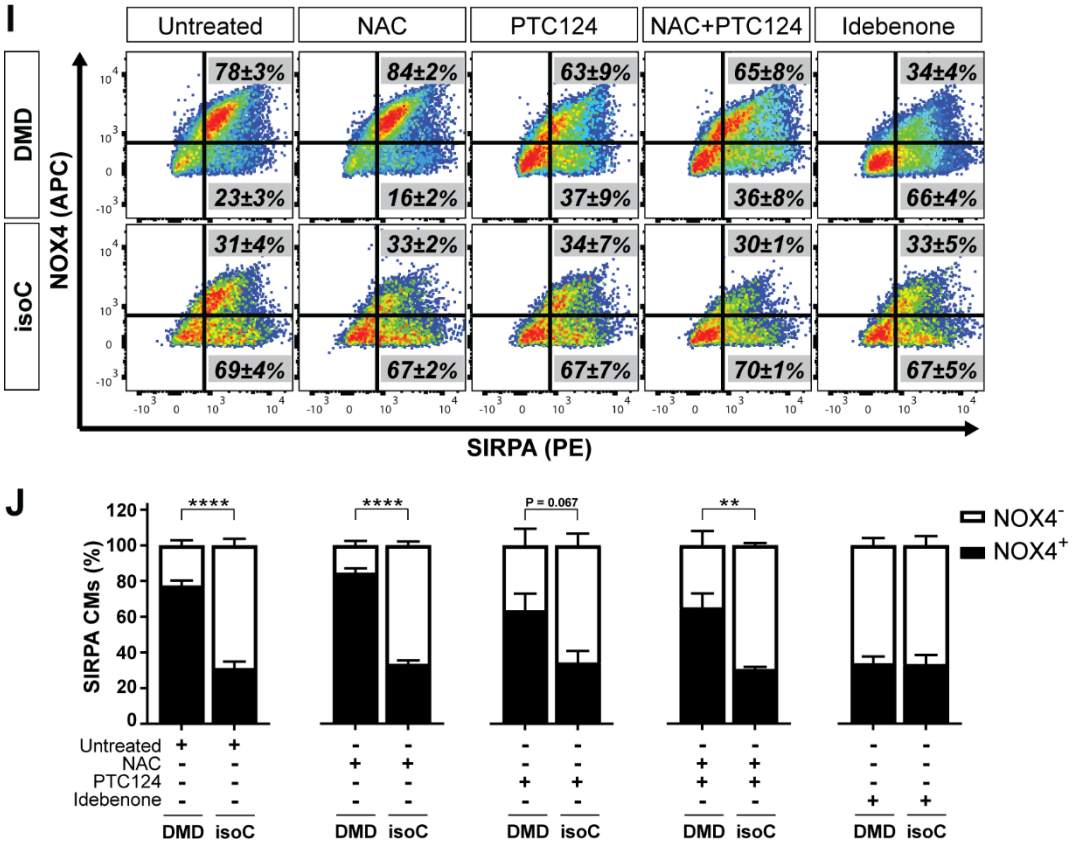

Fig. S4: Specificity of the treatment options on cell death and intracellular ROS concentrations, on $\Delta\Psi_m$ and mitochondrial superoxide concentrations, and on the expression levels of NOX4 in the experimental hiPSC-CM groups. (A) Example of flow cytometric analysis at day 15 of cardiac differentiation showing the percentage of cell death (using annexin V, APC and 7AAD, PerCP-Cy5) upon treatment in SIRPA (PE) positive hiPSC-CMs derived from DMD and DMD isogenic controls. **(B)** Corresponding flow cytometric quantification for cell death observed after the treatment options. **(C)** Representative flow cytometric analyses showing intracellular ROS concentrations in DMD and DMD isogenic hiPSC-CMs. **(D)** Quantification of the corresponding flow cytometric analyses showing the intracellular ROS levels. Data were representative of four independent experiments (n = 4). Data were reported as mean ± SEM; *p < 0.05; **p < 0.01; ***p < 0.001 and ****p < 0.0001. **(E)** Representative flow cytometric analyses at day 15 of cardiac differentiation for JC-1 aggregates (PE) and JC-1 monomers (FITC) upon treatment in DMD hiPSC-CMs and the DMD isogenic counterpart. **(F)** Corresponding flow cytometric quantification for $\Delta\Psi_m$. **(G)** Flow cytometric analyses at day 15 of differentiation showing the mitochondrial superoxide production (MitoSOX, PE) in depolarized DMD mitochondria. **(H)** Quantification of the corresponding flow cytometric analyses showing the mitochondrial superoxide production (MitoSOX). Data were representative of four independent experiments (n = 4). Flow cytometry data were reported as mean ± SEM; *p < 0.05; **p < 0.01; ***p < 0.001 and ****p < 0.0001. **(I)** Example of flow cytometric analysis at day 15 of cardiac differentiation showing the percentage of NOX4 (APC) on SIRPA (PE) positive DMD and DMD isogenic hiPSC-CMs upon the treatment options. **(J)** Corresponding flow cytometric quantification for NOX4. Data were representative of three independent experiments (n = 3). Flow cytometry data were reported as mean ± SEM; *p < 0.05; **p < 0.01; ***p < 0.001 and ****p < 0.0001.

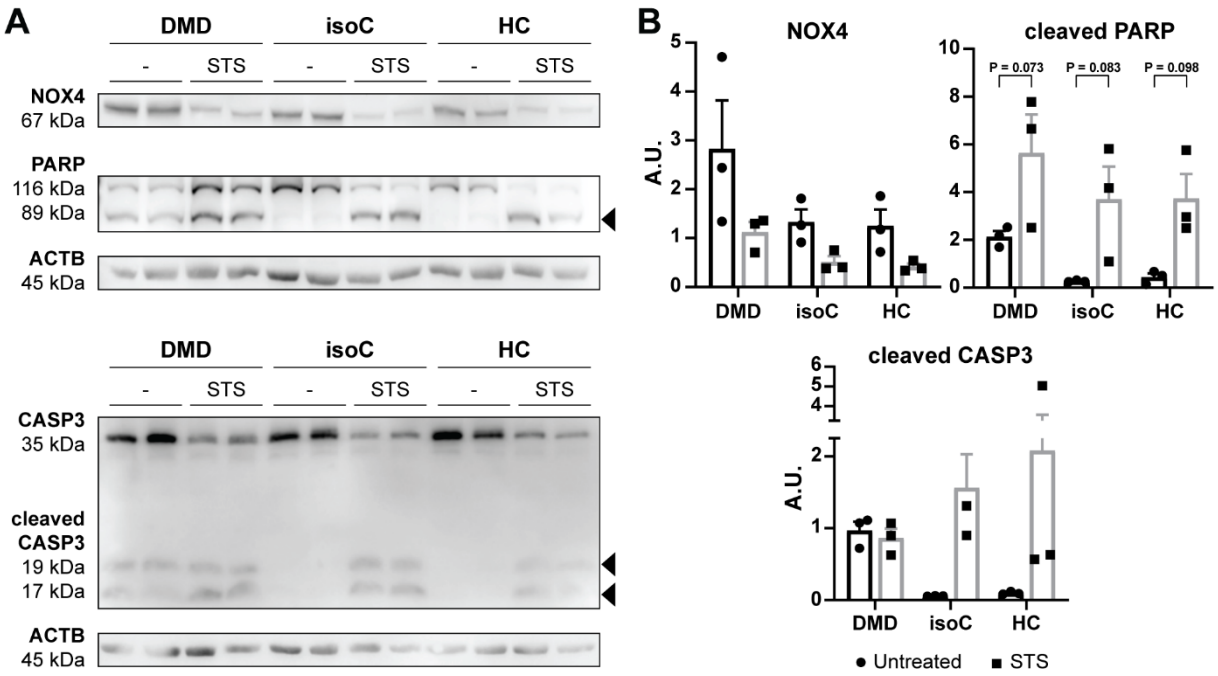

Fig. S5: NOX4 protein expression levels after STS-induced cell death in DMD and control hiPSC-CMs. (A) Western blot analysis showing cardiac NOX4 proteins and the cell death markers Poly (ADP-ribose) polymerase (PARP) and Caspase-3 (CASP3) in DMD and control hiPSC-CMs after a 6 h exposure to 1 μM STS. Cleaved forms of PARP and CASP3 are indicated by black triangles. ACTB was used as loading control. **(B)** Quantification of the western blot analysis for the markers NOX4, cleaved PARP and cleaved CASP3. Data were representative of three independent experiments (n = 3) and values were expressed as mean ± SEM.

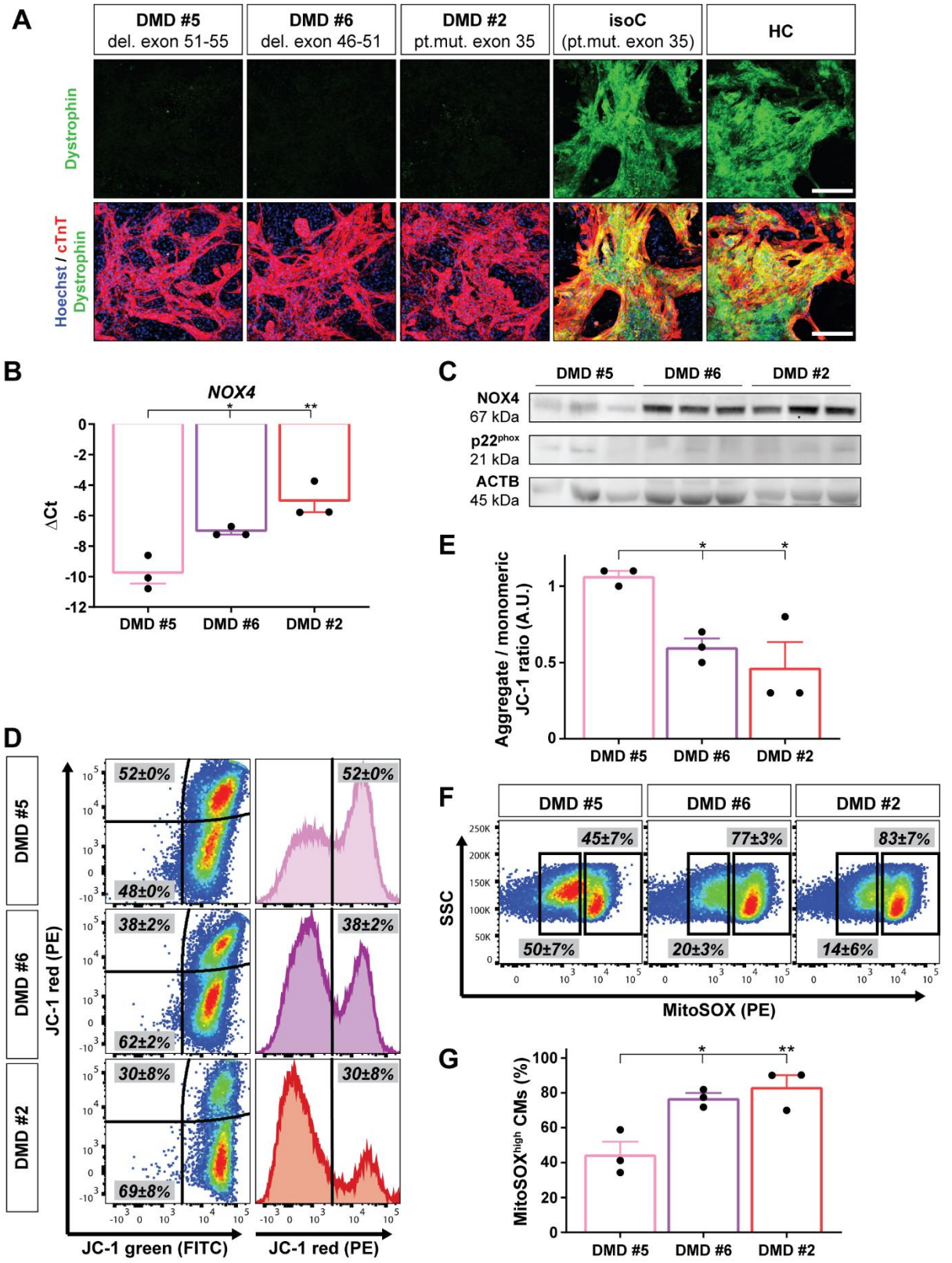

Fig. S6: Characterization of the DMD patient-specific hiPSC-CMs *in vitro*, showing increased NOX4 gene and protein expression levels, depolarized mitochondria and increased intracellular ROS levels. (A) Immunostaining showing the Dystrophin protein expression levels (green) in cTnT positive hiPSC-CMs (cTnT, red and Hoechst, blue), derived from three DMD patient subjects (DMD #2: pt. mut. exon 35; DMD #5: del. exon 51-55 and DMD #6: del. exon 46-51) and controls (see also Table S1). Scale bar = 100 μm. **(B)** *NOX4* mRNA levels in hiPSC-CMs of three DMD patients at day 8 of cardiac differentiation. Each data point was represented as ΔCt, normalized for the housekeeping genes

(*GAPDH* and *RPL13a*). Data were representative of three independent experiments (n = 3) and values were expressed as mean ± SEM; *p < 0.05; **p < 0.01; ***p < 0.001 and ****p < 0.0001. **(C)** Western blot analysis quantifying the corresponding NOX4 protein levels and its regulatory subunit $p22^{phox}$, normalized to the loading protein ACTB. **(D)** Representative flow cytometric analyses at day 15 of differentiation for JC-1 aggregates (PE) and JC-1 monomers (FITC) in three DMD patient-specific hiPSC-CMs. **(E)** Corresponding flow cytometric quantification of JC-1 aggregates and JC-1 monomers. **(F)** Flow cytometric analyses at day 15 of differentiation showing the mitochondrial superoxide production (MitoSOX, PE) in depolarized DMD mitochondria. **(G)** Corresponding flow cytometric quantification for the number of CMs with high mitochondrial superoxide concentrations. Data were representative of three independent experiments (n = 3). Flow cytometry data were reported as mean ± SEM; *p < 0.05; **p < 0.01; ***p < 0.001 and ****p < 0.0001.

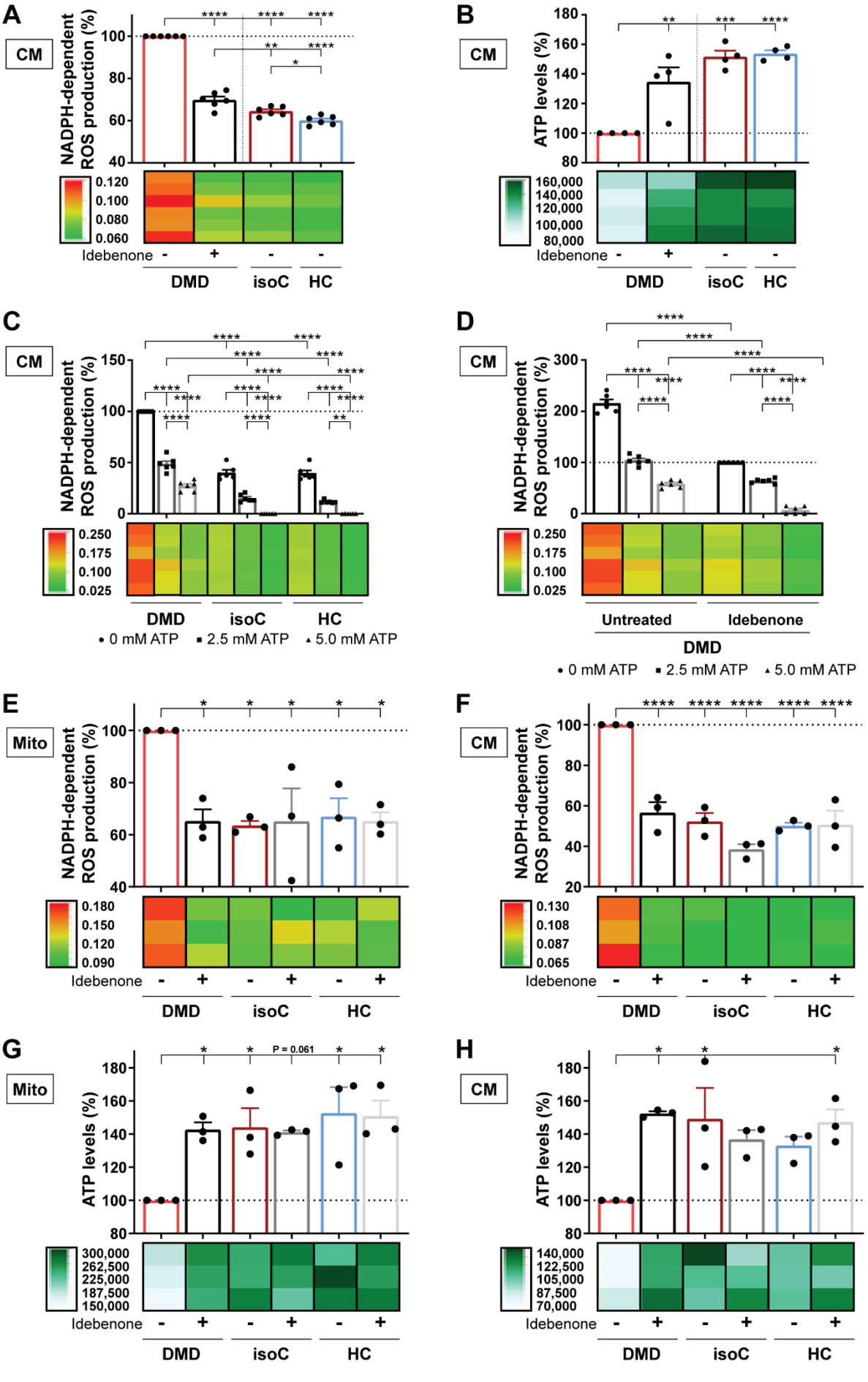
A
CM
NADPH-dependent ROS production (%)
Idebenone
DMD
isoC
HC
B
CM
ATP levels (%)
C
CM
NADPH-dependent ROS production (%)
DMD
isoC
HC
• 0 mM ATP ▪ 2.5 mM ATP ▲ 5.0 mM ATP
D
CM
NADPH-dependent ROS production (%)
Untreated
Idebenone
DMD
• 0 mM ATP ▪ 2.5 mM ATP ▲ 5.0 mM ATP
E
Mito
NADPH-dependent ROS production (%)
F
CM
NADPH-dependent ROS production (%)
G
Mito
ATP levels (%)
P = 0.061
H
CM
ATP levels (%)

Fig. S7: NADPH-dependent ROS production and intracellular ATP levels in DMD hiPSC-CMs after idebenone application, and the specificity of idebenone on the NADPH-dependent ROS production and ATP levels in the experimental hiPSC-CM groups. (A) Quantification of the NADPH-dependent superoxide production of NOX4 in the total CM fraction of DMD hiPSC-CMs with or without idebenone addition compared to controls. **(B)** ATP luminescence detection showing the effect of idebenone treatment on the intracellular ATP levels in DMD hiPSC-CMs. **(C)** Quantification of the ROS-producing NOX4 activity after 2.5 and 5.0 mM ATP addition in DMD hiPSC-CM and control cultures. Each data point was represented as percentage (%), normalized to the total CM fraction of the untreated DMD hiPSC-CMs. **(D)** Quantification of the NADPH-dependent superoxide production of NOX4 in the total CM fraction of DMD hiPSC-CMs upon 2.5 and 5.0 mM ATP addition, with or without idebenone treatment. Each data point was represented as percentage (%), normalized to the total CM fraction of the idebenone-treated DMD hiPSC-CM cultures. Data were representative of four or six independent experiments (n = 4 or n = 6) and values were expressed as mean ± SEM; *p < 0.05; **p < 0.01; ***p < 0.001 and ****p < 0.0001. Colored rectangles represented the independent experiments. Quantification of the NADPH-dependent superoxide production of NOX4 in the mitochondrial **(E)** and CM fraction **(F)** of hiPSC-CMs derived from DMD, DMD isogenic and healthy controls with or without idebenone treatment. **(G-H)** ATP luminescence detection showing the effect of idebenone treatment on the ATP levels in hiPSC-CMs cultures. Each data point was represented as percentage (%), normalized to the untreated DMD hiPSC-CM cultures. Data were representative of three independent experiments (n = 3) and values were expressed as mean ± SEM; *p < 0.05; **p < 0.01; ***p < 0.001 and ****p < 0.0001. Colored rectangles represented the independent experiments.

Table S1: Characteristics of DMD subjects and hiPSC lines.

	ID	DMD #2	DMD #5	DMD #6	DMD #2 isogenic	HC #1	HC #2	HC #3
	Origin	hFs	hPBMCs	hPBMCs	DMD #2	hPBMCs	hFs	hFs
	Mutation	pt.mut. exon 35 (c.4,996C > T; p.Arg1,666X)	del. exon 51-55	del. exon 46-51	CRISPR-Cas9 correction pt.mut. exon 35	NA	NA	NA
	Category	diseased	diseased	diseased	healthy	healthy	healthy	healthy
Phenotype	**Age start steroids**	7.5 years	4.5 years	6.5 years	NA	NA		
Phenotype	**Age loss of ambulation**	8.5 years	10 years	11 years				
Cardiomyopathy	**FS < 30%**	yes, 29%	no, 32%	no, 32%				
Cardiomyopathy	**EF**	50%	66%	61%				
Cardiomyopathy	**Measured at age**	20 years	9 years	20 years				
Cardiomyopathy	**Age at onset**	10 Years	NA	NA				
Pulmonary function	**FVC < 50%**	yes, 7%	no, 80%	yes, 19%				
Pulmonary function	**Measured at age**	25 years	9 years	19 years				

All DMD and control lines were previously characterized in-house or already published.
In the current study, somatic cells from DMD subjects were used to generate three diseased hiPSC lines DMD #2, DMD #5 and DMD #6 (Patel et al., 2019). Four different human control lines were used: (1) the DMD isogenic control line was in-house generated through CRISPR-Cas9 gene editing, as described in Materials and Methods; (2) HC #1 is commercially available from Thermo Fisher Scientific (Catalog number A18945); (3) HC #2 was kindly provided by Prof. C. Verfaillie (University of Leuven, Belgium) and generated by transduction of the new-born male fibroblast BJ1 cell line, as published by Coll et al. (Coll et al., 2018); and (4) HC #3 was a gift from Prof. P. Jennings (Medizinische Universität Innsbruck, Austria) to Prof. C. Verfaillie and generated by SeV-based reprogramming of male donor fibroblasts (SBAD2), as published by Rauch et al. (Rauch et al., 2018).
DMD: Duchenne muscular dystrophy; HC: healthy control; hPBMCs: human peripheral blood mononuclear cells; hFs: human fibroblasts; FS: fractional shortening; EF: ejection fraction; FVC: forced vital capacity; NA: not applicable.

Table S2: List of primers for Quantitative Real-Time PCR.

Gene	Primer direction	Primer sequence (5' > 3')
c-MYC	forward	TCCTCGGATTCTCTGCTCTCCT
	reverse	AGAAGGTGATCCAGACTCTGACCT
Dystrophin	forward	ATGCTTTGGTGGGAAGAAGT
	reverse	GGGCATGAACTCTTGTGGAT
GAPDH	forward	TCAAGAAGGTGGTGAAGCAGG
	reverse	ACCAGGAAATGAGCTTGACAAA
GDF-3	forward	ACACCTGTGCCAGACTAAGATGCT
	reverse	TGACGGTGGCAGAGGTTCTTACAA
HPRT	forward	TGACACTGGCAAAACAATGCA
	reverse	GGTCCTTTTCACCAGCAAGCT
hTERT	forward	AAATGCGGCCCCTGTTTCT
	reverse	CAGTGCGTCTTGAGGAGCA
KLF-4	forward	CGGACATCAACGACGTGAG
	reverse	GACGCCTTCAGCACGAACT
MALAT1	forward	GGACTTGCCTCAACTCCCTC
	reverse	GCCCTCTCAGCCACTCAAAT
MYH6	forward	GCCCTTTGACATTCGCACTG
	reverse	CGGGACAAAATCTTGGCTTTGA
MYH7	forward	ACTGCCGAGACCGAGTATG
	reverse	GCGATCCTTGAGGTTGTAGAGC
MYL2	forward	TTGGGCGAGTGAACGTGAAAA
	reverse	CCGAACGTAATCAGCCTTCAG
MYL7	forward	ACATCATCACCCACGGAGAAGAGA
	reverse	ATTGGAACATGGCCTCTGGATGGA
NANOG	forward	TGGCCGAAGAATAGCAATGGTGTG
	reverse	TTCCAGGTCTGGTTGCTCCACATT
NOX2	forward	TGCCAGTCTGTCGAAATCTGC
	reverse	ACTCGGGCATTCACACACC
NOX4	forward	TCCGGAGCAATAAGCCAGTC
	reverse	CCATTCGGATTTCCATGACAT
OCT4	forward	CGAGCAATTTGCCAAGCTCCTGAA
	reverse	GCCGCAGCTTACACATGTTCTTGA
p22^{phox}	forward	TACTATGTTCGGGCCGTCCT
	reverse	CACAGCCGCCAGTAGGTA
p47^{phox}	forward	GGGGCGATCAATCCAGAGAAC
	reverse	GTACTCGGTAAGTGTGCCCTG
p67^{phox}	forward	CCAGAAGCATTAACCGAGACAA
	reverse	CCTCGAAGCTGAATCAAGGC
RAC1	forward	ATGTCCGTGCAAAGTGGTATC
	reverse	CTCGGATCGCTTCGTCAAACA
RAC2	forward	TCTGCTTCTCCCTCGTCAG
	reverse	TCACCGAGTCAATCTCCTTGG
RAC3	forward	CTTCGAGAATGTTCGTGCCAA
	reverse	CCGCTCAATGGTGTCCTTG
REX1	forward	TGGAGGAATACCTGGCATTGACCT
	reverse	AGCGATTGCGCTCAGACTGTCATA
RPL13a	forward	CCTGGAGGAGAAGAGGAAAGAGA
	reverse	TTGAGGACCTCTGTGTATTTGTCAA
SOX2	forward	TGGCGAACCATCTCTGTGGT
	reverse	CCAACGGTGTCAACCTGCAT
TNNI1	forward	CCCAGCTCCACGAGGACTGAACA
	reverse	TTTGCGGGAGGCAGTGATCTTGG
TNNI3	forward	GATGCGGCTAGGGAACCTC
	reverse	GCATAAGCGCGGTAGTTGGA

Table S3: List of antibodies for flow cytometry (FC), immunostaining (IF) and western blot (WB).

Protein	Antibody name (#catalog number)	Provider	FC	IF	WB
ACTA2	Anti-Alpha Smooth Muscle Actin (Mouse monoclonal) **(#A2547)**	Merck		1:300	
ACTB	Beta Actin (13E5) (Rabbit monoclonal) **(#4970)**	Cell Signaling Technology			1:1,000
ACTN2	Anti-Sarcomeric Alpha Actinin (EA-53) (Mouse monoclonal) **(#ab9465)**	Abcam			1:100
AFP	Anti-Human Alpha-1-Fetoprotein (Rabbit polyclonal) **(#A0008)**	Dako		1:150	
Annexin V	APC Annexin V **(#550474)**	BD Pharmingen	1:20		
CASP3 (cleaved)	Cleaved Caspase-3 (Asp175) (Rabbit polyclonal) **(#9661)**	Cell Signaling Technology			1:500
CASP3 (full length)	Caspase-3 (Rabbit polyclonal) **(#9662)**	Cell Signaling Technology			1:1,000
cTnT	Recombinant Anti-Cardiac Troponin T (EPR3696) (Rabbit monoclonal) **(#ab92546)**	Abcam		1:100	
p22^{phox}	Anti-Cytochrome b245 Light Chain/p22-phox (44.1) (Mouse monoclonal) **(#ab80896)**	Abcam			1:100
Dystrophin (DMD)	DYS1 (Rod Domain) (Mouse monoclonal) **(#NCL-DYS1)**	Leica Novocastra		1:25	
Dystrophin (DMD)	DYS2 (C-terminus) (Mouse monoclonal) **(#NCL-DYS2)**	Leica Novocastra		1:25	
Dystrophin (DMD)	DYS3 (N-terminus) (Mouse monoclonal) **(#NCL-DYS3)**	Leica Novocastra		1:25	
LIN28	LIN-28 (S-15) (Goat polyclonal) **(#sc-54032)**	Santa Cruz Biotechnology		1:50	
NANOG	Nanog (Rabbit polyclonal) **(#PA1-097)**	Thermo Fisher Scientific		1:200	
NOX4	Anti-NADPH Oxidase 4 (Rabbit monoclonal) **(#ab133303)**	Abcam	1:2,175		1:1,000
OCT4	Anti-Oct4 - Embryonic Stem Cell Marker (Goat polyclonal) **(#ab27985)**	Abcam		1:200	
PARP	PARP (46D11) (Rabbit monoclonal) **(#9532)**	Cell Signaling Technology			1:1,000
SIRPA	PE Anti-Human CD172a/b (SIRPα/β) **(#323806)**	BioLegend	1:100		
SOX2	Sox-2 (Y-17) (Goat polyclonal) **(#sc-17320)**	Santa Cruz Biotechnology		1:50	
SSEA4	SSEA-4 (MC813) (Mouse monoclonal) **(#sc-59368)**	Santa Cruz Biotechnology		1:50	
TRA-1-60	TRA-1-60 (TRA-1-60) (Mouse monoclonal) **(#sc-21705)**	Santa Cruz Biotechnology		1:50	
TUBB	Beta Tubulin (Rabbit monoclonal) **(#NB110-57610)**	NovusBio		1:250	

SUPPLEMENTAL EXPERIMENTAL PROCEDURES

Study design and ethics statement

The objective of this study is to develop a stem cell-based model to investigate pathological mechanisms and evaluate their therapeutical potential in cardiomyopathy in DMD patients. The study was conducted in compliance with the principles of the Declaration of Helsinki, the principles of 'Good Clinical Practice' (GCP) and in accordance with all applicable regulatory requirements. The use of human samples from healthy control donors and DMD subjects for experimental purposes and protocols in the present study was approved by the Ethics Committee of the University Hospitals Leuven (respectively, S55438 and S65190). Subjects information, used in this study, is summarized in Table S1.

Chemicals and reagents

NAC (Merck), ataluren (PTC124; Selleckchem) and idebenone (Santhera Pharmaceuticals, Pratteln Switzerland). STS (Merck). CM-H_2DCFDA Total Intracellular ROS Indicator, JC-1 Mitochondrial Membrane Potential Probe, MitoSOX Red Mitochondrial Superoxide Indicator and MitoTracker-Red CMXRos Mitochondria Probe (all from Thermo Fisher Scientific). ATP Solution, Luminescent ATP Detection Assay Kit, Colorimetric NADPH Assay Kit (both from Abcam) and Mitochondrial Isolation Kit for Cultured Cells (Thermo Fisher Scientific).

Generation of integration-free DMD hiPSCs

hFs and hPBMCs were isolated from DMD patients with known *Dystrophin* mutations (Table S1). Somatic cells were reprogrammed towards pluripotency using the integration-free SeV-based technology, performed according to the manufacturer's instructions (CytoTune-iPS 2.0 Sendai Reprogramming Kit; Thermo Fisher Scientific).

Teratoma formation assay

Pluripotency of SeV-reprogrammed hiPSCs was evaluated *in vivo* in 6- to 8-week-old immunodeficient *Rag2-null γc-null*/Balb/C mice. Teratoma formation experiments in mice were conducted following the guidelines of the Animal Welfare Committee of Leuven University and Belgian/European legislation (approved July 2016; P174/2016).

Generation of DMD isogenic control line through CRISPR-Cas9 genome editing

To restore full-length expression of the *Dystrophin* gene, the isogenic control for the DMD hiPSC patient line, characterized by a genetic point mutation in exon 35 (c.4,996C > T; p.Arg1,666X) of the *Dystrophin* gene, was generated through CRISPR-Cas9 from the *S. pyogenes* system (5'-NGG PAM) as previously described (Ran et al., 2013). Briefly, two 20-nucleotide sgRNAs (sgRNA #1: FW seq. CACCG-ATTTAACCACTCTTCTGCTC and RV seq. AAAC-GAGCAGAAGAGTGGTTAAAT-C; sgRNA #2: FW seq. CACCG-TAACCACTCTTCTGCTCAGG and RV seq. AAAC-CCTGAGCAGAAGAGTGGTTA-C) were designed and ligated into the RNA-guided nuclease plasmid (pX330-mCherry plasmid; Addgene), in order to induce the Cas9-mediated DSB in the genomic DNA of the Dystrophin-deficient hiPSCs. Cas9-mediated genome editing was performed via HDR. The targeted DNA modification required the use of a plasmid-based donor repair template with two homology arm regions for the *Dystrophin* gene, flanking a GFP-Hygromycin-TK expressing cassette for selection. Here, one of the homology arms contained the genetic correction of the nonsense mutation in the *Dystrophin* gene. Finally, a completely gene editing-free DMD isogenic hiPSC line was obtained due to PiggyBac excision and Fialuridine (FIAU; Merck) selection, restoring the expression of functional Dystrophin protein (Table S1).

Quantitative Real-Time PCR analysis

Total RNA was extracted using the PureLink RNA Mini Kit and treated with the TURBO DNA-Free DNase Kit to assure highly pure RNA. 1 μg RNA was reverse transcribed into cDNA with SuperScript III Reverse Transcriptase First-Strand Synthesis SuperMix. Quantitative Real-Time PCR was performed with the Platinum SYBR Green qPCR SuperMix-UDG (all from Thermo Fisher Scientific). The oligonucleotide primer sequences (all from IDT) are listed in Table S2. A 10-fold dilution series ranging from 10^{-3} to 10^{-8} of 50 ng/μL human genomic DNA was used to evaluate the primer efficiency. Delta Ct (ΔCt) values were calculated by subtracting the Ct values from the genes of interest with the Ct values of the housekeeping genes (*GAPDH, HPRT* and *RPL13a*).

Flow cytometric analysis

Differentiated hiPSC-CMs were dissociated using Collagenase A (1 U/mL) for 20 minutes at 37°C. All flow cytometry procedures were performed according to the manufacturer's instructions. Hank's

Balanced Salt Solution (HBSS; pH 7.2) with $CaCl_2$ and $MgCl_2$ supplemented with 2% FBS (both from Thermo Fisher Scientific), 10 mM HEPES and 10 mM NaN_3 (both from Merck), was used as staining buffer. For high CM purity, hiPSC-CMs were stained for the surface marker SIRPA (data not shown). If intracellular staining was necessary, cells were fixed with 4% paraformaldehyde (PFA; Polysciences) for 10 minutes at 37°C and permeabilized in ice-cold 90% methanol (Merck) for 30 minutes on ice, before the staining procedure. Fluorescence minus one (FMO) controls and compensations were included for appropriate gating. Samples were analyzed using the FACS Canto II HTS (BD Biosciences) and quantified using FlowJo Software Version 10 (FlowJo LLC). Table S3 provides a list of all flow cytometric antibodies used in this study.

Immunofluorescence imaging

Cells were fixed with 4% PFA for 10 minutes at 4°C, permeabilized for 30 minutes at room temperature in PBS supplemented with 0.2% Triton X-100 and 1% Bovine Serum Albumin (BSA) and blocked for 30 minutes at room temperature in 10% donkey serum (all from Merck). Samples were stained overnight at 4°C with the primary antibodies, followed by the appropriate secondary antibodies (1 h incubation at room temperature). Immunofluorescent primary and secondary antibodies were listed in Table S3. Nuclei were counterstained with 10 μg/mL Hoechst (33342; Thermo Fisher Scientific). Analyses were assessed using the Nikon Eclipse Ti Microscope or the Nikon Eclipse Ti A1R Configurated Confocal Microscope, with appropriate NIS-Elements Software (all from Nikon).

Mitochondria and cytoplasmic fractionation

Mitochondrial and cytoplasmic separation was performed using the Mitochondrial Isolation Kit for Cultured Cells (Thermo Fisher Scientific), according to the manufacturer's instructions with minor modifications. To obtain a more purified mitochondrial fraction (with a more than 50% reduction of the lysosomal and peroxisomal contaminants), the post-cell debris supernatant was subjected to an extra centrifuge step at 3000 x g for 15 minutes. For Western blot analysis, mitochondrial pellets were lysed with 2% CHAPS (Merck) in Tris-buffered saline (TBS; containing 25 mM Tris, 0.15 M NaCl; pH 7.2) and subsequently centrifuged at high speed for 2 minutes. Western blot analysis was performed on the supernatant, containing soluble mitochondrial protein.

Western blot analysis

Western blot analysis for cell lysates was performed in RIPA buffer supplemented with 10 mM NaF, 0.5 mM Na_3VO_4, 1:100 protease inhibitor cocktail and 1 mM Phenylmethylsulfonyl Fluoride (PMSF; all from Merck). Equal amounts of protein (40 μg) were heat-denaturated at 95°C in sample-loading buffer (50 mM Tris-HCl, 100 mM DTT, 2% SDS, 0.1% bromophenol blue and 10% glycerol; pH 6.8), resolved by SDS-polyacrylamide gel electrophoresis and subsequently transferred to nitrocellulose membranes (Amersham Protran Western Blotting Membranes; Merck). The filters were blocked with TBS containing 0.05% Tween and 5% non-fat dry milk (Merck). Incubation was done overnight with the indicated primary antibody dilutions, as listed in Table S2. Horseradish peroxidase-conjugated secondary antibodies (Bio-Rad) were diluted 1:5,000 in TBS-Tween (0.05%) with 2.5% non-fat dry milk. After incubation with SuperSignal Pico or Femto chemiluminescence substrate (both from Thermo Fisher Scientific), the polypeptide bands were detected with GelDoc Chemiluminescence Detection System (Bio-Rad). Quantification of relative densitometry was obtained by normalizing to the background and to loading control proteins (ACTB, from Cell Signaling Technology) using Image Lab Software (Bio-Rad).

Patch-clamp electrophysiology and Ca^{2+} recordings

Single cells were seeded on Matrigel-coated coverslips. Cells were perfused at 37°C with a solution containing the following (in mM): 137 NaCl, 5.4 KCl, 1.8 $CaCl_2$, 0.5 $MgCl_2$, 10 glucose and 10 Na-HEPES. The pH was adjusted to 7.4 with NaOH. The patch-clamp pipettes were filled with a solution containing the following (in mM): 120 K-Asp, 20 KCl, 10 HEPES, 5 Mg-ATP, 10 NaCl and 0.05 K_5Fluo-4. The pH was adjusted to 7.2 with KOH. Patch electrode resistances were between 2.5 and 3 MΩ when the pipettes were filled with intracellular solution. Cells were patched in the whole-cell configuration. Data were recorded using an Axopatch 200B amplifier (Axon Instruments) at a sampling rate of 10 kHz. Signals were filtered with 5 kHz low-pass Bessel filters. APs were recorded in current-clamp mode, and if not spontaneous, after a 5 ms pulse of 0.5 nA at a 1 Hz frequency. Ca^{2+} currents were measured in voltage-clamp mode. After a Na^+ current inactivation step from -70 mV to 40 mV for 750 ms, Ca^{2+} currents were recorded with 10 mV voltage steps from -40 mV to 60 mV during 205 ms. For analysis, the maximum amplitude of the Ca^{2+} current was measured and corrected for the cell capacitance. Data were analyzed with Clampfit Software (Axon Instruments).

Contractility measurements of 3D EHT constructs

The contractile properties of 3D EHTs were monitored by measuring the deflection distances of the microposts of the EHT device (in μm) during spontaneous contraction and relaxation under temperature-controlled conditions (37°C) in oxygenated Tyrode's solution (in mM; containing 137 NaCl, 5.4 KCl, 0.5 $MgCl_2$, 12.8 HEPES and 5.5 Glucose; dissolved in deionized sterile water at pH 7.4) with Ca^{2+}. A Ca^{2+} concentration of 1.8 mM was used to mimic physiological conditions. EHT constructs for contractility measurements were generated from 8-day-old hiPSC-CMs and monitored after 5 days of EHT maturation.

ATP luminescence detection

The levels of cellular ATP were measured using the Luminescent ATP Detection Assay Kit (Abcam), according to the manufacturer's instructions. The Luminescent ATP Detection Assay Kit is based on the production of light caused by the reaction of ATP with added firefly's luciferase and luciferin. The ATP concentration is proportional to the emitted light. Briefly, hiPSC-CMs (20,000 cells per well in 100 μL volume) were seeded in a 96-well white microplate. Next day, 50 μL of cell lysis solution was added to each well and the plate rotated for 5 minutes using an orbital shaker at 700 rpm to lyse cells and stabilize ATP. The plate was kept in the dark for 10 minutes and recordings were performed with the EG&G Berthold Microplate Luminometer LB 96V and corresponding software (Berthold Technologies) (Shanmugasundaram et al., 2017).

Measurements of NADPH-dependent ROS production

The Colorimetric NADPH Assay Kit (Abcam) provides a convenient method for detecting NADPH in contrast to the traditional NAD/NADH and NADP/NADPH assays (which monitor the changes in NADH or NADPH absorption at 340 nm, suffering low sensitivity and high interference) (Griendling et al., 2016). Here, the NADPH probe is a chromogenic sensor that has its maximum absorbance at 460 nm upon NADPH reduction. The absorption of the NADPH probe is directly proportional to the concentration of NADPH. NADPH-dependent ROS production was measured in the presence or absence of 2.5 or 5.0 mM ATP (preincubated for 60 minutes) in the total CM fraction or isolated mitochondrial fraction, according to the manufacturer's instructions. Briefly, hiPSC-CMs (20,000 cells per well in 100 μL volume) were seeded in a 96-well black microplate with clear flat bottoms. NADPH probe was added to samples and incubated for 30 minutes and protected from light. Recordings were performed with the ELx808 Absorbance Microplate Reader with absorbance measurements at 460 nm and quantified using Gen5 Software Version 3 (both from BioTek Instruments) (Sambon et al., 2020).

Statistical analysis

Data were statistically analyzed using Prism Software Version 8 (GraphPad). All data were reported as mean ± standard error of the mean (SEM). Differences between two groups were examined for statistical significance using Student's t-test. One-Way or Two-Way ANOVA (with multiple comparisons test and Tukey's or Bonferroni's correction) were used for three or more groups. Significance of the difference was indicated as follows: *$p < 0.05$; **$p < 0.01$; ***$p < 0.001$ and ****$p < 0.0001$.

SUPPLEMENTAL REFERENCES

Coll, M., Perea, L., Boon, R., Leite, S.B., Vallverdu, J., Mannaerts, I., Smout, A., El Taghdouini, A., Blaya, D., Rodrigo-Torres, D., et al. (2018). Generation of Hepatic Stellate Cells from Human Pluripotent Stem Cells Enables In Vitro Modeling of Liver Fibrosis. Cell Stem Cell *23*, 101-113 e107. 10.1016/j.stem.2018.05.027.

Griendling, K.K., Touyz, R.M., Zweier, J.L., Dikalov, S., Chilian, W., Chen, Y.R., Harrison, D.G., Bhatnagar, A., and American Heart Association Council on Basic Cardiovascular, S. (2016). Measurement of Reactive Oxygen Species, Reactive Nitrogen Species, and Redox-Dependent Signaling in the Cardiovascular System: A Scientific Statement From the American Heart Association. Circ Res *119*, e39-75. 10.1161/RES.0000000000000110.

Patel, A.M., Wierda, K., Thorrez, L., van Putten, M., De Smedt, J., Ribeiro, L., Tricot, T., Gajjar, M., Duelen, R., Van Damme, P., et al. (2019). Dystrophin deficiency leads to dysfunctional glutamate clearance in iPSC derived astrocytes. Transl Psychiatry *9*, 200. 10.1038/s41398-019-0535-1.

Ran, F.A., Hsu, P.D., Wright, J., Agarwala, V., Scott, D.A., and Zhang, F. (2013). Genome engineering using the CRISPR-Cas9 system. Nat Protoc *8*, 2281-2308. 10.1038/nprot.2013.143.

Rauch, C., Feifel, E., Kern, G., Murphy, C., Meier, F., Parson, W., Beilmann, M., Jennings, P., Gstraunthaler, G., and Wilmes, A. (2018). Differentiation of human iPSCs into functional podocytes. PLoS One *13*, e0203869. 10.1371/journal.pone.0203869.

Sambon, M., Gorlova, A., Demelenne, A., Alhama-Riba, J., Coumans, B., Lakaye, B., Wins, P., Fillet, M., Anthony, D.C., Strekalova, T., and Bettendorff, L. (2020). Dibenzoylthiamine Has Powerful Antioxidant and Anti-Inflammatory Properties in Cultured Cells and in Mouse Models of Stress and Neurodegeneration. Biomedicines *8*. 10.3390/biomedicines8090361.

Shanmugasundaram, K., Nayak, B.K., Friedrichs, W.E., Kaushik, D., Rodriguez, R., and Block, K. (2017). NOX4 functions as a mitochondrial energetic sensor coupling cancer metabolic reprogramming to drug resistance. Nat Commun *8*, 997. 10.1038/s41467-017-01106-1.